Accepted Manuscript

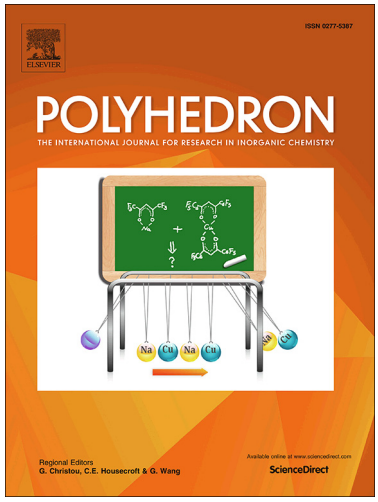

A Green and Cost-Effective Approach for the Production of Gold Nanoparticles Using *Corn Silk* Extract: A Recoverable Catalyst for Suzuki-Miyaura Reaction and Adsorbent for Removing of Dye Pollutants

Mohammad Mehdi Khodaei, Mahsa Dehghan

PII: S0277-5387(19)30082-8
DOI: https://doi.org/10.1016/j.poly.2019.01.060
Reference: POLY 13733

To appear in: *Polyhedron*

Received Date: 16 October 2018
Revised Date: 25 January 2019
Accepted Date: 27 January 2019

Please cite this article as: M.M. Khodaei, M. Dehghan, A Green and Cost-Effective Approach for the Production of Gold Nanoparticles Using *Corn Silk* Extract: A Recoverable Catalyst for Suzuki-Miyaura Reaction and Adsorbent for Removing of Dye Pollutants, *Polyhedron* (2019), doi: https://doi.org/10.1016/j.poly.2019.01.060

A Green and Cost-Effective Approach for the Production of Gold Nanoparticles Using *Corn Silk* Extract: A Recoverable Catalyst for Suzuki-Miyaura Reaction and Adsorbent for Removing of Dye Pollutants

Mohammad Mehdi Khodaei,[a,b]* Mahsa Dehghan[a]

[a] Department of Organic Chemistry, Razi University, Kermanshah 67149-67346, Iran.

[b] Nanoscience & Nanotechnology Research Center (NNRC), Razi University, Kermanshah 67149-67346, Iran

* Corresponding author. Tel.: +98-83-34277605. Fax: +98-83-34274759. E-mail address: mmkhoda@razi.ac.ir (M. M. Khodaei)

Abstract

In this study, we have developed an eco-friendly and inexpensive method for the synthesis of gold nanoparticles immobilized on the Schiff-base functionalized SBA-15 by using of *Corn silk* extract as a natural reducing agent. Appropriate analyses confirm the structure of this heterogeneous nanocomposite. This synthesized nanocomposite acts as a robust nanocatalyst for the selective production of biphenyls in Suzuki-Miyaura coupling reaction and a strong adsorbent for degradation of anionic and cationic dyes such as methyl orange and methylene blue. The results show that this composite leads to the formation of biphenyl derivatives in excellent yields even for less-active aryl halides such as chlorobenzene at mild conditions and efficient degradation of organic dyes (>99%) in a short time through a pseudo-first order kinetic model. Easy separation of this nanocomposite from the reaction mixture by applying an external magnet and its reusability for several times without significant loss in its activity, are the other advantages of this nanocomposite.

Keywords: Corn silk extract; Nanoadsorbent; Magnetic; Suzuki-Miyaura reaction; Organic dyes.

1. Introduction

In recent years, metal nanoparticles have attracted a lot of attention due to their unique characteristics such as high activity, higher fermi potential, excellent performance and applications as active catalyst for many electron-transfer reactions [1-7]. There are different methods for the production of metal nanoparticles including photocatalytic and chemical reduction of metal salts [4,6,7], and solvent extraction [5]. An alternative, efficient and green method to the chemical methods is plant extract [8].

Corn silk refers to the shiny and weak fibers that grow as a part of ears of corn. It is a waste material in the cultivation of corn. Corn (maize) can be cultivated in the most parts of the world [9]. For the first time, the Native Americans [10] and Chinese [11] used the *corn silk* extract as an effective herb. Now, many developed countries use it as a traditional medicine. It contains proteins, carbohydrates, vitamins, minerals and fiber [12]. *Corn silk* extract has shown positive therapeutic effects in a number of cases such as bladder infections, inflammation of the urinary system, inflammation of the prostate, kidney stones, bedwetting, diabetes, high blood pressure and high cholesterol levels [13-25]. Its therapeutic potential is related to the presence of bioactive components especially flavonoids and terpenoids. Flavonoids (polyphenols) are an important class of natural antioxidants [26]. Therefore, *corn silk* can act as a strong, natural and safe reducing agent for the production of metal nanoparticles.

In recent years gold nanoparticles have been used for catalyzing of various organic reactions such as oxidation, reduction and hydrochlorination reactions [27-29] Several research works present in which Au NPs have been used for coupling reactions [37-39]. Common catalysts for Suzuki-Miyaura coupling reaction include palladium, nickel [30], and copper [31] complexes. Some examples show that gold (I) complexes are strong catalysts for coupling reactions [32]. For high efficiency, ease of separation and reusability, these complexes immobilize on solid supports as nanoparticles [33-36]. Herein, we demonstrate that gold nanoparticles immobilized on mesoporous silica can efficiently catalyze Suzuki coupling reaction. The SBA-15 materials, with thick walls (around 4 nm), allow easier entry of substrates to the inner surface of the materials, which accelerates the physical and chemical processes [40-44]. The modification of SBA-15 with different organic compounds improves its features [44,45]. There is a large number of catalytic applications of Schiff-base functionalized SBA-15. The Schiff-base derivatives have different properties; hence, they can be used in different fields such as organic and bioinorganic chemistry, catalyst, synthesis of various compounds and liquid crystal. The existence of electron pair on the

nitrogen atom with the ability to coordinate to metal ions or different organic groups makes Schiff-bases highly flexible in the synthesis and modifications [46-52].

In this research, Au NPs prepare with a simple, cost-effective and nontoxic method by using of *Corn silk* extract as a natural reducing agent and then, immobilize on the Schiff-base functionalized SBA-15 (Fe_3O_4-Au@SF-SBA-15). This magnetically separable nanocomposite plays a dual role as a nanocatalyst for Suzuki-Miyaura coupling reaction and a nanoadsorbent for rapid degradation of cationic and anionic dyes. Herein, we report the catalytic role of Au NPs for coupling reactions between aryl halides and arylboronic acids for the production of biaryl compounds in excellent yields even for less-reactive aryl halides such as chlorobenzene derivatives. In this research, the final catalyst (Fe_3O_4-Au@SF-SBA-15) was characterized by FESEM, CHN, EDX, Mapping, TEM, FT-IR, BET/BJH, TGA, low-angle and wide-angle XRD techniques (Scheme 1).

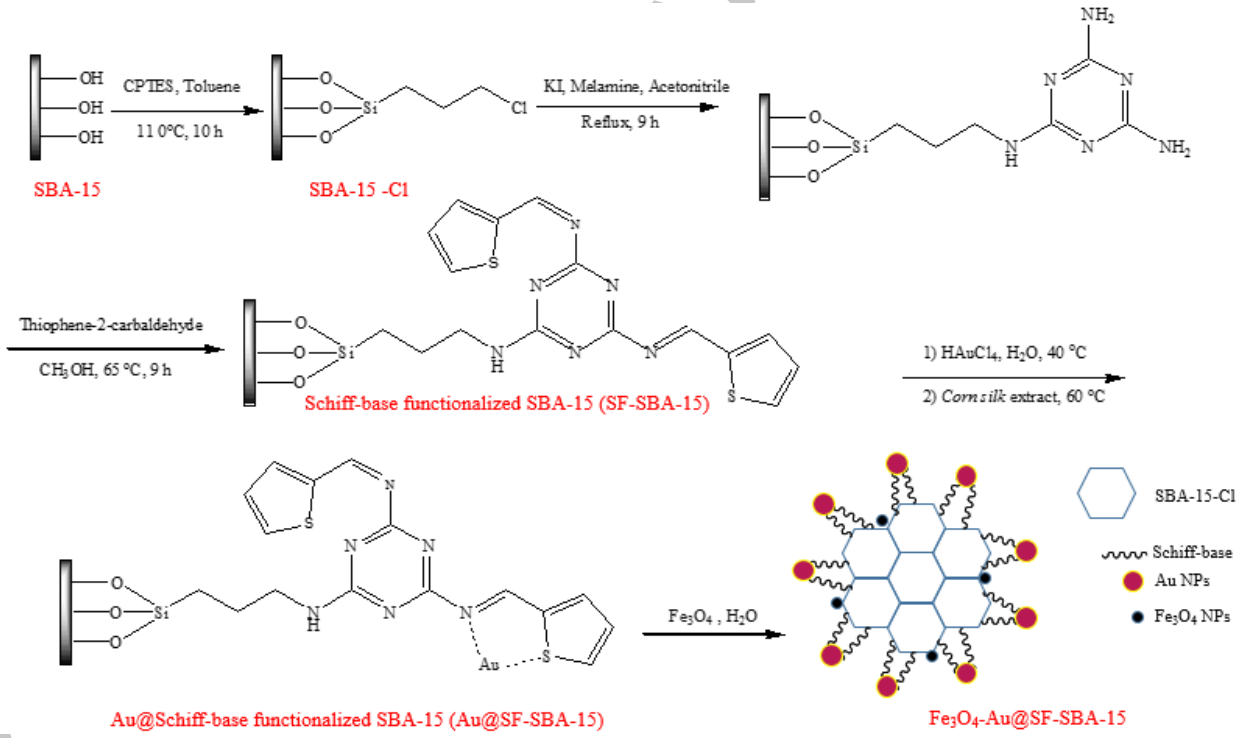

Scheme 1: Preparation of Au NPs immobilized on the Schiff-base functionalized SBA-15 (Fe_3O_4-Au@SF-SBA-15).

2. Experimental section

2.1. Apparatus and instruments

A BRUKER ALPHA spectrophotometer was used to record FT-IR spectra (range: 400-4000 cm^{-1}). An X'PertPro diffractometer using Cu Kα radiation acquired the X–ray diffraction patterns. Transmission electron microscopy (TEM) analysis was performed using a ZEISS-EM 10C at 80 kV acceleration voltage. Field emission Scanning electron microscopy (FESEM, Mapping) and EDX were performed on a ZEISS SIGMA VP-500 instrument. N_2 adsorption-desorption isotherms were measured at -196 ^{o} C using BELSORP-mini II instrument. Thermogravimetric analysis (TGA) was carried out using an STA PT- 1000 instrument at a heating rate of 10 ^{o} C min^{-1} in air. The concentration of Au was estimated using inductively coupled plasma optical emission spectrometer (ICP-OES) Varian Vista PRO Radial.

2.2. Chemicals and materials

Pluronic P123 (Ethylene Oxide-Propylene Oxide-Ethylene Oxide), Mw = 5800 g/mol, tetraethyl orthosilicate (TEOS), 3-chloropropyl triethoxysilane (CPTES, 99%), 1,3,5- triazine- 2,4,6- triamine (melamine), 2-thiopene carbaldehyde, hydrogen tetrachloroaurate tetrahydrate, methyl orange (MO), methylene blue (MB), aryl halide derivatives, phenylboronic acid derivatives, potassium carbonate, ethanol and hydrochloric acid were supplied by Merck and Aldrich companies and were used without further purification. Double distilled water was used throughout the experiments.

2.3. Synthesis of Schiff-base functionalized SBA-15 (SF-SBA-15)

The SBA-15 support was prepared through surfactant method by Zhao et al. [53,54]. Then, it was modified by Vunain et al. method [55]. Briefly, the amount of 50 mL of dry toluene, 5.0 g of SBA-15 and 5.0 mL (20.76 mmol) of 3-chloropropyl triethoxysilane (CPTES) were introduced to a 100 mL of round-bottom flask. This solution was refluxed for 24 h and then, the solid (SBA-15-Cl) was filtered and washed with toluene, dichloromethane, and methanol, and dried at 110 ^{o} C [56]. At the next step, we added the amount of 0.83 g (5.0 mmol) of potassium iodide to a solution of 1.0 g of SBA-15-Cl in 50 mL of acetonitrile at 50 ^{o} C. After 1 h, 0.63 g (5.0 mmol) of melamine was added and then, refluxed for 9 h. Then, we filtered the obtained solid, rinsed with ethanol and dried at 80 ^{o} C. After that, the obtained solid that was produced in previous step (1.0 g) was dissolved in 50 mL of methanol and 1.24 g (11.0 mmol) of 2-thiophenecarbaldehyde was added to it and refluxed for 9 h. After completion of the reaction, the obtained product (SF-SBA-15) was separated.

2.4. Extraction of *corn silk* extract

We use a simple procedure for the extraction of *corn silk* extract. We poured the fresh *corn silks* (10.0 g) in a 500 mL beaker containing 200 mL of deionized water. Then, we heated this mixture at 60 ^{o}C for 8 h. After that, we separated the *corn silks* by filtration and placed the filtrate at room temperature until the whole of its water evaporates and a concentrated substance (like honey) remains.

2.5. Synthesis of Au@SF-SBA-15

For the synthesis of Au@SF-SBA-15, we added the amount of 0.2 g of SF-SBA-15 to an aqueous solution of $HAuCl_4$ (1 mM) and stirred for 24 h at 40 ^{o}C. Then, the temperature was increased from 40 ^{o}C to 60 ^{o}C and 4 mL of *corn silk* extract (2.5% W/V) added to the solution and stirred for 1 h. We separated the obtained solid, washed several times with deionized water and dried. The loading of Au was measured to be 2.54 wt% by ICP-OES.

2.6. Synthesis of Fe_3O_4-Au@SF-SBA-15

In a 100 mL round-bottom flask, the as-prepared Fe_3O_4 NPs (0.1 g) was dispersed in 20 mL of absolute ethanol by ultra-sonication (Fe_3O_4 NPs were synthesized by using of the method described in our previous work) [57]. In another 100 mL round-bottom flask, 0.1 g of Au@SF-SBA-15 was added to 40 mL of ethanol and stirred for 30 min at ambient temperature. Then, we added the dispersed Fe_3O_4 NPs to this solution and stirred for 24 h. After that, we isolated the solid product by an external magnet and dried at 50 ^{o}C.

2.7. Adsorption experiments

The performance of synthesized nanocomposite investigated by the degradation of MO and MB in the presence of $NaBH_4$ as a source of hydride ion. All experiments were done at ambient temperature as follow: $NaBH_4$ aqueous solution (2 mL, 0.25 M) was added into aqueous solutions of MO and MB (18 mL, 50 ppm) under stirring. Then, the amount of 1.0 mg of Fe_3O_4-Au@SF-SBA-15 nanoadsorbent (0.013 mmol% of Au) was dispersed in the above solution and changes of the absorption peaks in UV-Vis spectrometer were recorded. In order to evaluate the effect of the variables on the adsorption of organic dyes, the effect of pH (5.0-9.0), the amount of adsorbent (1.0-3.0 mg) and contact time (10-300 sec) were investigated. The pH adjusted by adding aqueous solutions of HCl (0.1 M) or NaOH (0.1 M). The concentrations of MO and MB solutions analyzed

by measuring their absorbance at 464 and 553 nm, respectively. These wavelengths correspond to the maximum absorption peaks of MO and MB dyes. Calibration curves obtained by using of standard solutions of MO and MB with known concentrations versus the absorbance. The results of calibration experimental data were shown as a straight line with a high coefficient of determination (R^2 = 0.999). The amount of absorbed dyes by the adsorbent and the adsorption percentage calculate by the following equations [58]:

$$q = ((C_0 - C_e)\ V)/m \qquad [1]$$

$$\%\ \text{adsorption} = (100\ (C_0 - C_e))\ /\ C_0 \qquad [2]$$

Where q is the amount of absorbed dyes on per gram of adsorbent (mg/g), C_0 and C_e are the initial and equilibrium concentrations of dyes in aqueous solutions (mg/L), respectively, V is the initial volumes of dye solutions (L), and m is the mass of the adsorbent (g).

2.8. General procedure for Suzuki–Miyaura coupling reaction

A mixture of aryl halide (1 mmol), phenylboronic acid (1.2 mmol), K_2CO_3 (2 mmol), Fe_3O_4-Au@SF-SBA-15 nanocatalyst (50 mg or 0.64 mmol% of Au) and 5 mL of C_2H_5OH/H_2O (1:1) were added to a 25 mL round-bottom flask and stirred at 80 ^{o} C for appropriate times. After completion the reaction (controlled by TLC), the mixture was cooled and the catalyst was recovered by a magnet and washed three times with ethyl acetate and ethanol. The combined organic layer was dried over $MgSO_4$. Then the solvent was evaporated and the residue was purified by column chromatography and characterized by its ^{1}H NMR, ^{13}C NMR and melting point.

3. Results and discussion

3.1. Characterization of Fe_3O_4-Au@SF-SBA-15

XRD patterns of Fe_3O_4 NPs (a), Au@SF-SBA-15 (b), and Fe_3O_4-Au@SF-SBA-15 (c) present in Figure 1. In Figure 1a, the strong peaks at 2θ = 30.2°, 36.4°, 43.7°, 53.5°, 56.3°, 62.3°, and 73.8° are attributed to the (220), (311), (400), (422), (511), (440) and (533) planes of highly crystalline cubic spinel structure of Fe_3O_4 NPs [59,60] (JCPDS no. 19–0629). In Figure 1b, a broad peak at 2θ = 23° is attributed to the amorphous silica walls [61] and diffraction peaks at 2θ = 38.4°, 44.2°, 64.3°, and 77.7^{o} are corresponded to the (111), (200), (220) and (311) planes of metallic Au NPs (JCPDS no. 04-07834). The same sets of characteristic peaks in Figures 1a and 1b are also

observed for Fe_3O_4-Au@SF-SBA-15 indicating the presence and stability of the crystalline phase of Fe_3O_4 and Au NPs on the amorphous silica walls (Figure 1c).

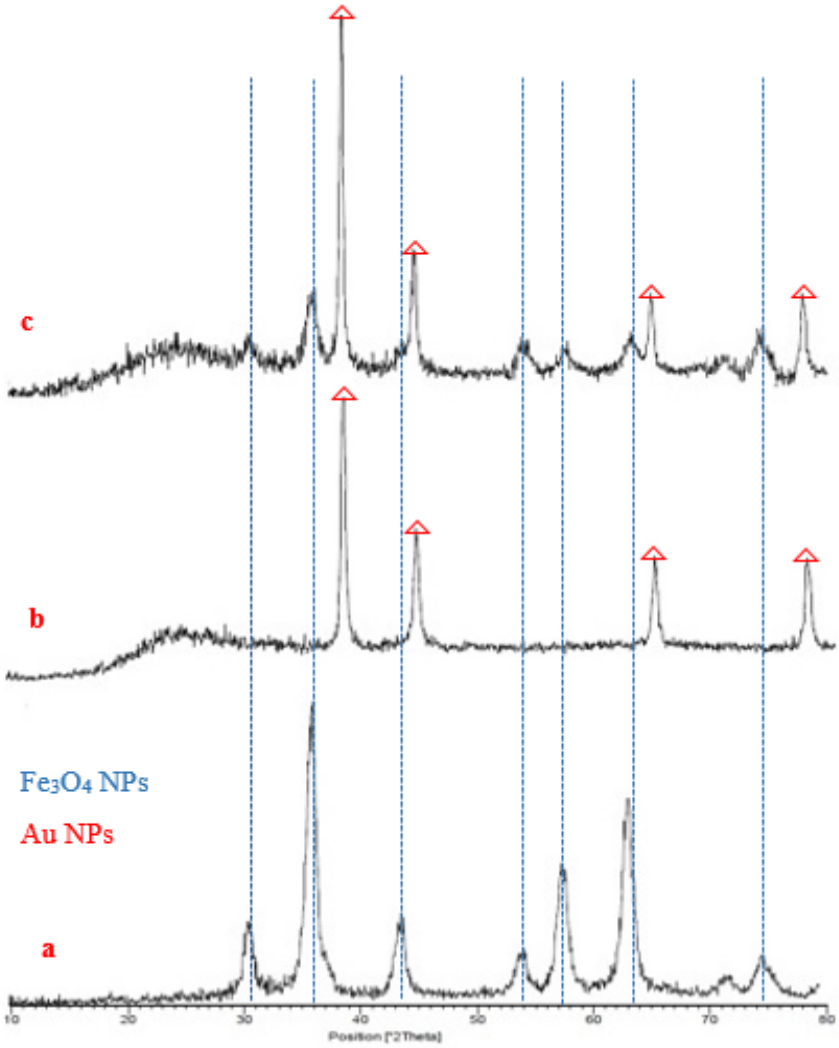

Figure 1: The XRD patterns of the Fe_3O_4 NPs (a), Au@SF-SBA-15 (b) and Fe_3O_4-Au@SF-SBA-15 (c).

The low-angle X-ray scattering measurement can effectively identify the mesoporous materials with hexagonal symmetry. Figure 2 shows the low-angle XRD pattern of Fe_3O_4-Au@SF-SBA-15. It can be observed that the three distinct reflections for Fe_3O_4-Au@SF-SBA-15 in the low-angle region indexed as (100), (110) and (200), are exactly same as reflections for SBA-15 [62]. This

observation proves that the ordered hexagonal mesoporous structure of SBA-15 preserves its structure after Schiff-base functionalization and immobilization of Au NPs.

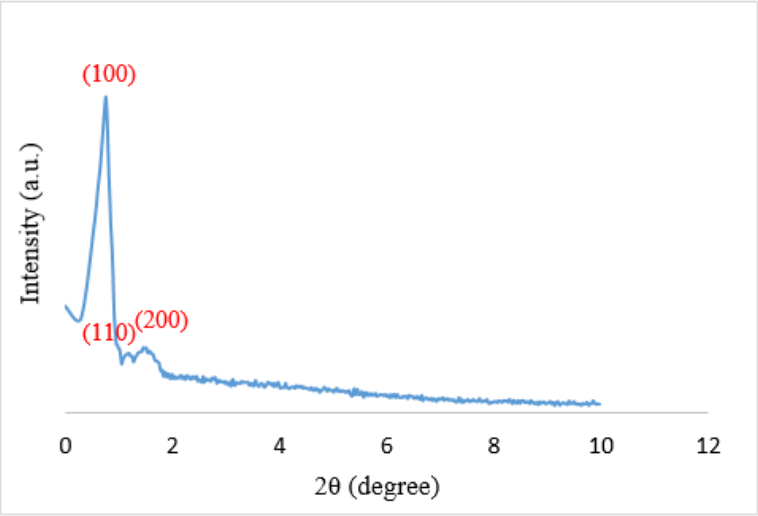

Figure 2: Low-angle XRD spectrum of Fe_3O_4-Au@SF-SBA-15.

ICP and EDS analyses confirm the presence of Au units in the Fe_3O_4-Au@SF-SBA-15 nanocomposite. FESEM and TEM images can characterize the morphology of the synthesized nanocomposite. TEM images clearly showed the presence of well-ordered two-dimensional hexagonal mesoporous for the SBA-15 (Figure 3a), Au@SF-SBA-15 (Figure 3b) and Fe_3O_4-Au@SF-SBA-15 (Figure 3c). TEM images for Au@SF-SBA-15 and Fe_3O_4-Au@SF-SBA-15 show that Au and Fe_3O_4 NPs have been well-dispersed on the surface of SBA-15 and suggests that the SBA-15, despite the loading of metal NPs has sufficient structural stability to retain its morphology. Small black dots, observed in the TEM images in Figure 3b and 3c, are assigned to Au(0) NPs [63] and bigger black dots in the TEM image of Fe_3O_4-Au@SF-SBA-15 (Figure 3c) that have not appeared in the TEM image of Au@SF-SBA-15 (Figure 3b), are attributed to Fe_3O_4 NPs.

The FESEM images of SBA-15 and Fe_3O_4-Au@SF-SBA-15 are shown in Figure 3d-f. As can be seen in Figure 3d, the FESEM of SBA-15 sample consists of short rods with wheat like morphologies and rod-like structures that randomly packed bunch. In addition, these types of morphologies have long-range parallel channels with two-dimensional hexagonal structures. The

morphology of SBA-15 after functionalization with Schiff-base and immobilization of Au NPs is same as the SBA-15 (Figures 3e and 3f). The Mapping analysis and EDX pattern of Fe_3O_4-Au@SF-SBA-15 show the presence of Au, C, N, O and S atoms, which it suggests that successful grafting and immobilizing of Schiff-base and Au NPs on the surface of SBA-15 support.

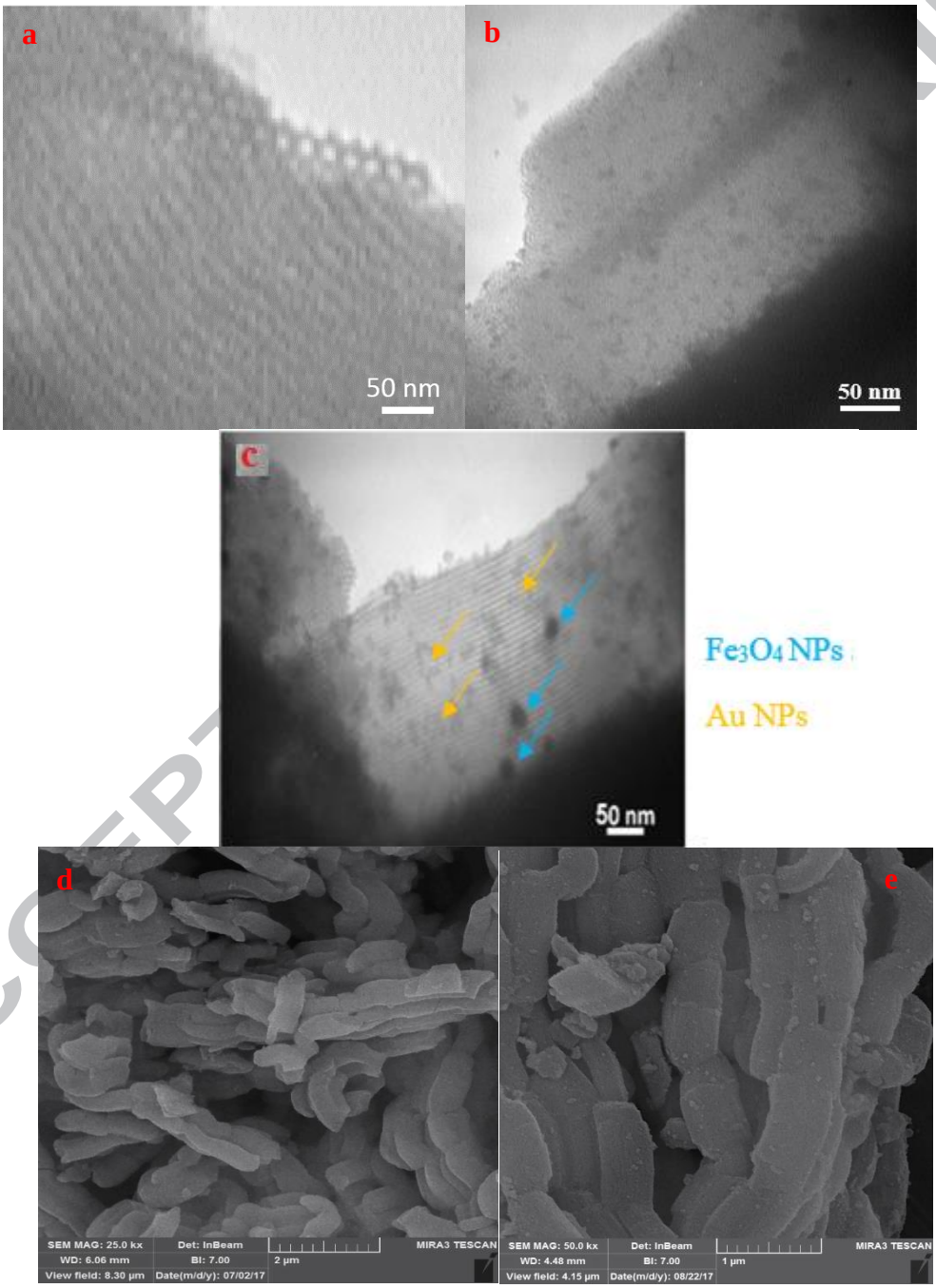

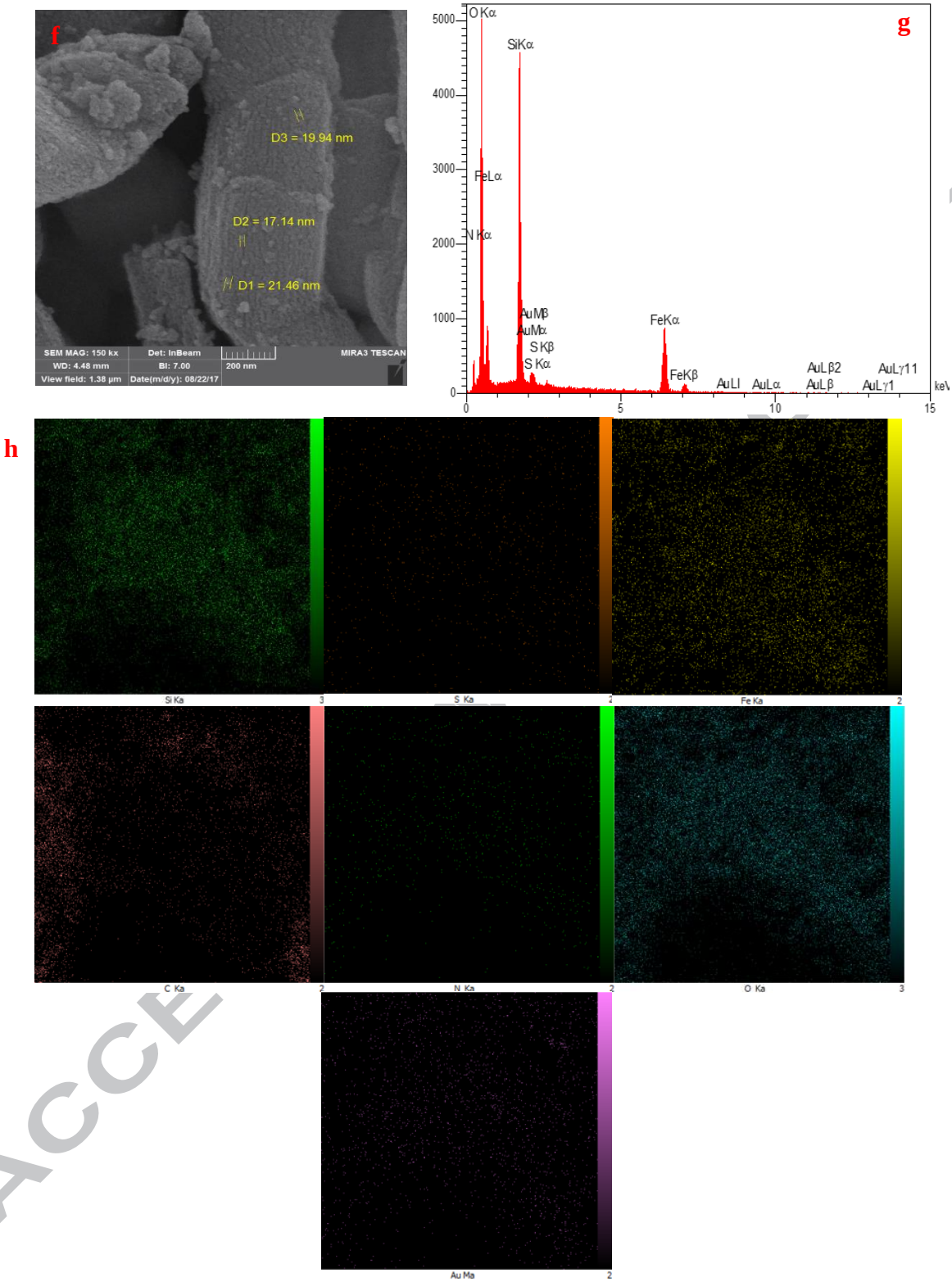

Figure 3: TEM images of SBA-15 (a), Au@SF-SBA-15 (b) and Fe_3O_4-Au@SF-SBA-15 (c) and FESEM images of SBA-15 (d) and Fe_3O_4-Au@SF-SBA-15 (e,f), EDX pattern of Fe_3O_4-Au@SF-SBA-15 (g) and mapping analysis of Fe_3O_4-Au@SF-SBA-15 (h).

In a comparative mode, the FT-IR spectra for each step of the synthesis of introduced nanocomposite (Fe_3O_4-Au@SF-SBA-15) are available in Figure 4a-f. The broad band at 3450 cm^{-1} in Figure 4a is assigned to O—H stretching of silanol groups and the adsorbed water molecules. The stretching and bending vibrations of Si–O–Si can be detected at 1100 and 800 cm^{-1}, respectively. The weak peaks at 2990 and 2850 cm^{-1} in Figure 4b-e are assigned to the methylene group vibrations in the propyl chain. The appeared peak at around 1640 cm^{-1} is attributed to the characteristic vibration of imine group of N-(thiophen-2-ylmethylene)-1,3,5-triazine-2,4,6-triamine, while this band shifts to lower frequency (1630 cm^{-1}) in the Au@SF-SBA-15 catalyst (Figure 4d). The shifting of this band to lower frequency confirmed the formation of metal–ligand bonds. In addition, the band at 1540 cm^{-1} is assigned to aromatic —C=C— stretching vibration. Figure 4e exhibits a characteristic peak at 579 cm^{-1}, which is attributed to the Fe-O stretching vibration that the existence of this peak proves the presence of Fe_3O_4 NPs in the synthetic nanocomposite. These results indicate that the organic moieties are successfully grafted to the SBA-15. The FT-IR spectrum of *corn silk* extract presents in Figure 4f. *Corn silk* contains proteins, carbohydrates, vitamins, minerals, and fiber. *Corn silk* is rich of flavonoids [64]. Flavonoids are strong anti-oxidants. The presence of flavonoids in the *corn silk* can be proven qualitatively through FT-IR spectroscopy. The FT-IR spectrum in Figure 4(f) shows the following characteristic peaks: 3418, 2930, 2870, 1611, 1389 and 1050 cm^{-1}, respectively. The appeared peaks at 3418, 2930 and 2870 cm^{-1} are related to the OH group and the symmetric stretching vibration of CH_2. The peak at 1611 cm^{-1} is assigned to the stretching vibration of —C=C— and the other peak at 1389 cm^{-1} is corresponded to the phenolic OH. The appeared peak at 1050 cm^{-1} is attributed to the stretching vibration of C-H, which is specific for the aromatic nucleus [65].

The N_2 adsorption/desorption isotherms for SBA-15, SF-SBA-15 and Fe_3O_4-Au@SF-SBA-15 are shown in Figure 5. The textural properties present in Table 1. As can be seen in Figure 5, all materials show a type IV standard IUPAC isotherm hysteresis loop at a high relative pressure values (P/P_0 = 0.65) [66]. It is a characteristic of mesoporous materials with a narrow pore size distribution [67]. However, their shapes are different, with a capillary condensation of N_2 occurring over a slightly lower P/P_0 range when going from SBA-15 to Fe_3O_4-Au@SF-SBA-15 nanoadsorbent [68]. With the same order for the adsorbed N_2 volume, the pore volumes decrease. The data of the isotherms with the correlation coefficient from BET fitting are used to calculate the physicochemical properties of the materials. The reduction in the specific surface area and pore

size of functionalized SBA-15 compare to SBA-15 can be attributed to the presence of Schiff-base, Au and Fe_3O_4, which blocks the channels (Table 1)

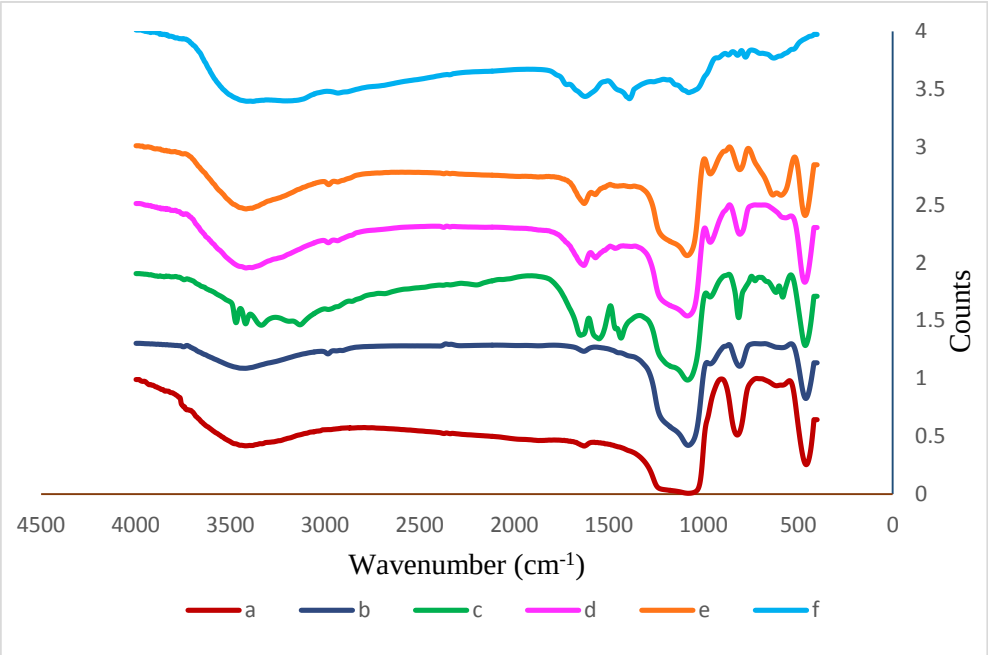

Figure 4: FT-IR spectra of SBA-15 (a), SBA-15-Cl (b), SF-SBA-15 (c), Au@SF-SBA-15 (d), Fe_3O_4-Au@SF-SBA-15 (e) and *corn silk* extract (f).

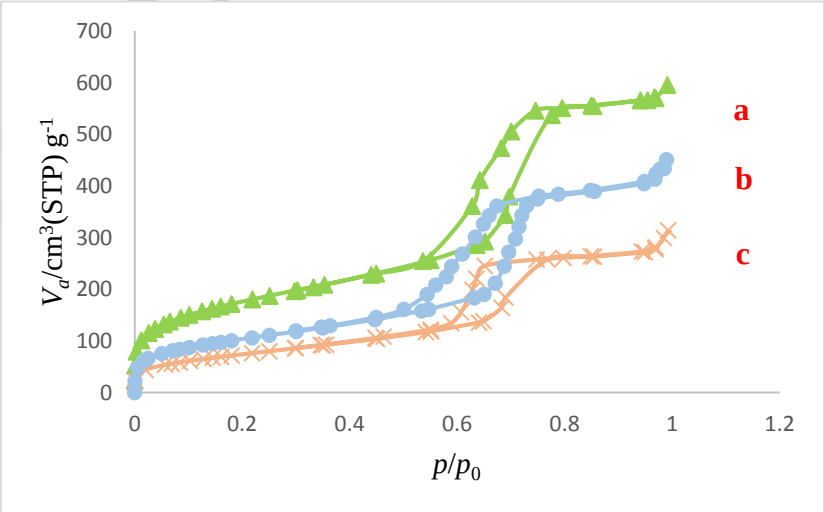

Figure 5: N_2 adsorption-desorption isotherm curves for SBA-15 (a), SF-SBA-15 (b) and Fe_3O_4-Au@SF-SBA-15 (c).

Table 1: Specific surface area, pore volume and mean pore diameters for SBA-15, SF-SBA-15 and Fe_3O_4-Au@SF-SBA-15 nanocomposite.

Materials	Surface area (m^2g^{-1})[a]	Pore volume (cm^3g^{1-})[b]	Pore diameter (nm)[c]
SBA-15	622.63	0.92	7.69
SF-SBA-15	363.75	0.70	7.00
Fe_3O_4-Au@SF-SBA-15	274.12	0.48	5.90

[a] S_{BET}
[b] Total pore volume determined at $P/P_0 = 0.99$.
[c] Mean pore diameter determined using the BJH method.

UV-Vis spectroscopy is a useful tool for investigating formation of gold NPs in the presence of *corn silk* extract. As can be seen in Figure 6, the appeared peak at 550 nm after reduction of $HAuCl_4$ by the plant extract indicates the formation of Au NPs [69].

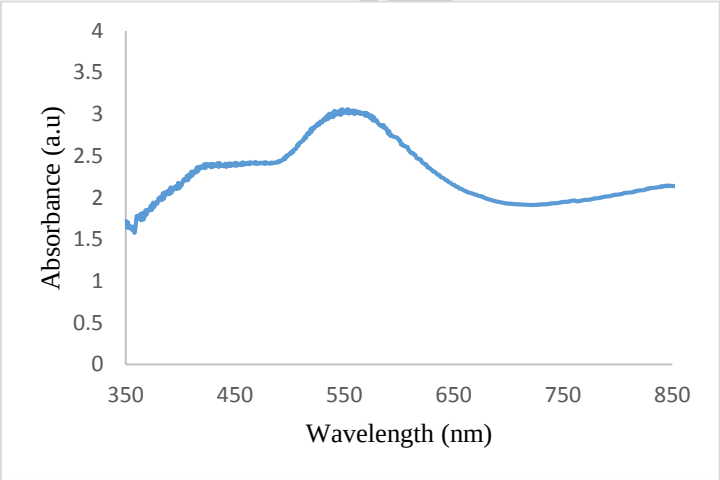

Figure 6: UV-Vis spectrum of reduction of $HAuCl_4$ in the presence of *corn silk* extract.

The thermogravimetric analysis of SF-SBA-15 and Fe_3O_4-Au@SF-SBA-15 nanocomposite presents in Figure 7. The initial weight losing before 100 ^oC might be attributed to the elimination of physically adsorbed water. The new step of the weight losing for SF-SBA-15 between 240-620 ^oC (39.4%) and for Fe_3O_4-Au@SF-SBA-15 between 100-600 ^oC (14.53%) could be attributed to the decomposition of organic templates. As can be seen, by the incorporation of Fe_3O_4 and Au NPs, the weight losing decreased from 39.4% to 14.53% because of the increasing of inorganic

content in the Fe_3O_4-Au@SF-SBA-15. Another step of weight losing after 600 ^{o}C is due to the decomposition of silanol groups [70].

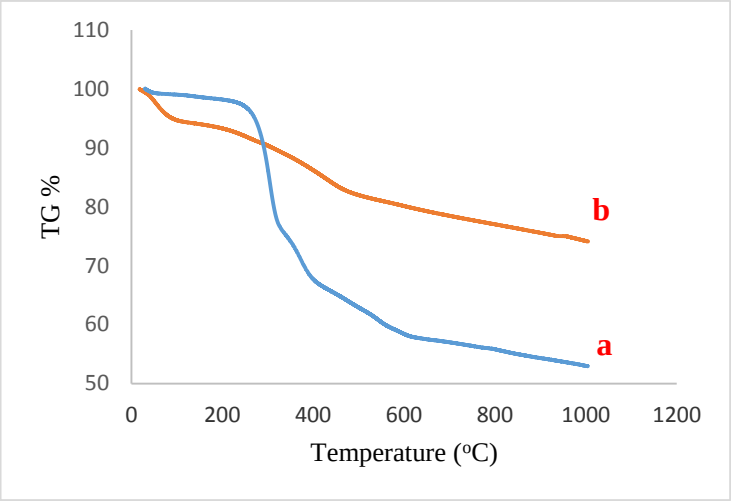

Figure 7: TG curves of SF-SBA-15 (a) and Fe_3O_4-Au@SF-SBA-15 (b).

Elemental analysis (CHN) of bulk catalysis (Fe_3O_4-Au@SF-SBA-15) shows the percentage of C, H, N, S and O atoms. In addition, the amounts of Fe and Au were measured by ICP-OES analysis. The results present in Table 2.

Table 2: Elemental analysis for Fe_3O_4-Au@SF-SBA-15 nanocomposite.

C	H	N	S	O	Au	Fe
4.63%	2.02%	2.41%	1.58%	9.45%	2.54%	8.59%

3.2. Evaluation of the catalytic performance for the adsorption of dye molecules

MO and MB as the typical organic pollutants were selected to evaluate the catalytic performance of the Fe_3O_4-Au@SF-SBA-15 with $NaBH_4$ as reducing agent. $NaBH_4$ was used, since it has high electron injection capacity of the BH_4^-. Due to the high importance of removing of dye pollutants from the environment, many researchers have focused their attention on this issue [71-77].

In the absence of adsorbent or reducing agent, the degradation efficiency is very low and after 2 h no significant changes of the peaks at 464 and 553 were observed (Figure 8a and 8b). In addition,

in the presence of SF-SBA-15 with or without $NaBH_4$ no significant changes of the peaks apperceived. This suggest that neither the nanocatalyst nor $NaBH_4$ alone is able to catalyze the swift degradation of dye molecules. Green plots in Figure 8 show the role of Fe_3O_4 NPs in the adsorption process. Based on the obtained results in the absence of magnetic NPs, complete degradation of MO and MB happens. The amount of Fe_3O_4 NPs in the adsorbent (Fe_3O_4-Au@SF-SBA-15) is much less than that play a significant role in degradation process. A little amount of Fe_3O_4 NPs only added to functionalized SBA-15 just for easy separating of nanoadsorbent at the end of the reaction.

Based on the obtained results in Figures 8c and 8d, the degradation of organic dyes could be complete quickly when both Fe_3O_4-Au@SF-SBA-15 and $NaBH_4$ exist together. This observed enhancement of the catalytic efficiency relates to the relaying of electrons from BH_4^- to MO and MB *via* the Au NPs [78]. Therefore, the Fe_3O_4-Au@SF-SBA-15 nanocomposite has superior catalytic activity for adsorbing of these dye molecules. Figure 9 shows the kinetic curves for the reduction of MO and MB by Fe_3O_4-Au@SF-SBA-15 nanoadsorbent. The linear variation of $\ln(C_t/C_0)$ versus reaction time indicates that the reaction follows pseudo-first-order kinetics, where C_0 and C_t represent the concentration of the organic dyes after time 0 and t, respectively [79]. According to the formula $\ln(C_t/C_0) = -kt$, the apparent rate constants k (sec^{-1}) estimated from the slopes of straight lines for MO and MB are 0.0137 and 0.0133 sec^{-1}, respectively.

Three independent variables (pH, the amount of adsorbent and contact time) show the effect of reaction variables on the degradation of MO and MB. There are the range and levels of the variables in Table S1 (see supporting information). Twenty experiments were designed and the Removal % of dyes were measured as the process responses. The results and experimental conditions present in Tables S2 and S3 for MO and MB, respectively. The ANOVA tables (Analysis of Variance) for effective variables on catalyst function for degradation of MO and MB are presented in Tables S4 and S5, respectively. The significance of each of the independent variables evaluates by F-value and P-value tests. Significant model terms and meaningful interactions are those that P-value for them is less than 0.05. So, it is deduced from Table S4, A, B, C, A^2, C^2, AC and BC with P-value < 0.05 are significant model terms or the most effective variables on catalyst function for degradation of MO (A: pH, B: the amount of adsorbent and C: contact time). Also, based on Table S5, the most effective variables on catalyst function for degradation of MB are A, C, A^2, AB and BC. Surface and contour plots related to meaningful

interactions present in Figures S1-S4. Adjusted R-squared for degradation of MO and MB is almost up to 99%, which shows that the proposed model for investigating the Removal % of dyes is very suitable. Equations 3 and 4 state the relationship between meaningful experimental variables and process responses for MO and MB, respectively (the constant value and the coefficients for effective variables are available in Tables S4 and S7 in supporting information).

$$Y = -501.57+154.97A+9.68B+0.898C-11.15A^2-0.001C^2-0.051AC-0.0126BC \quad [3]$$

$$Y = -552.58+158.64A-0.260C-9.665A^2-2.830AB+0.052BC \quad [4]$$

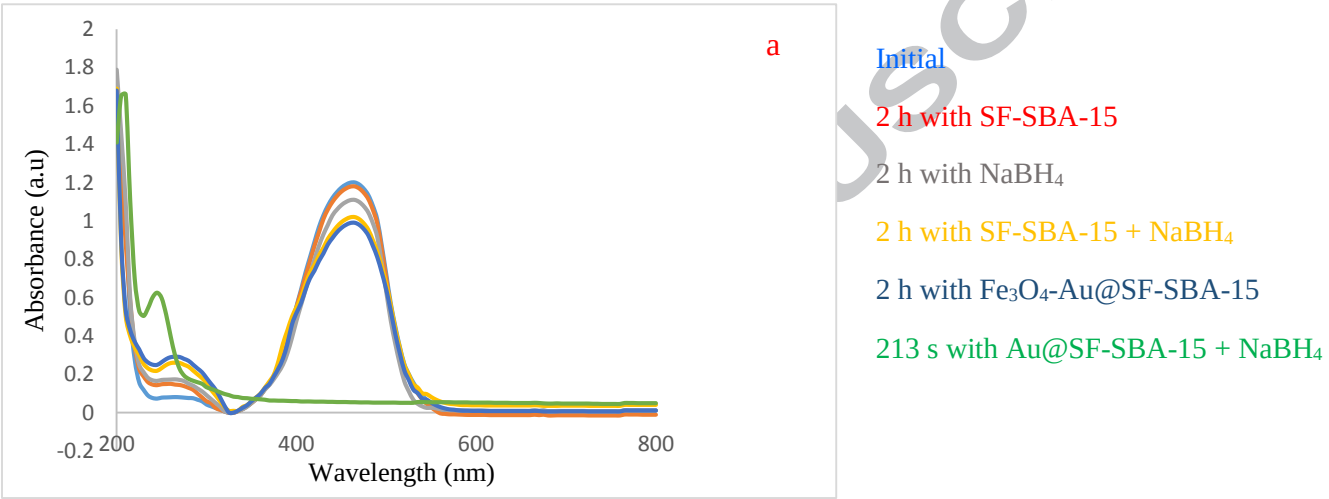

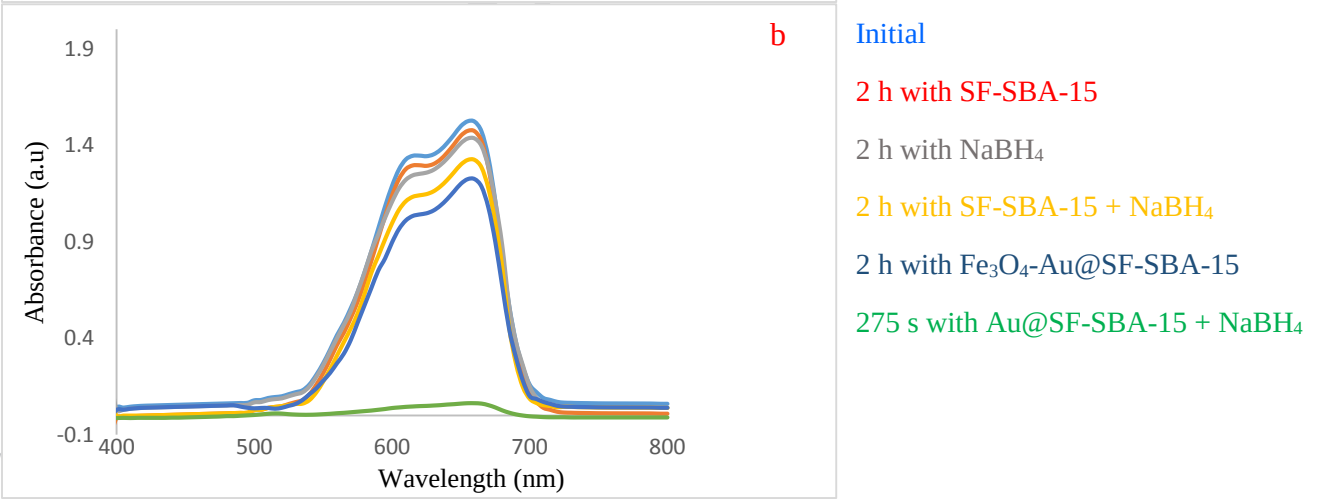

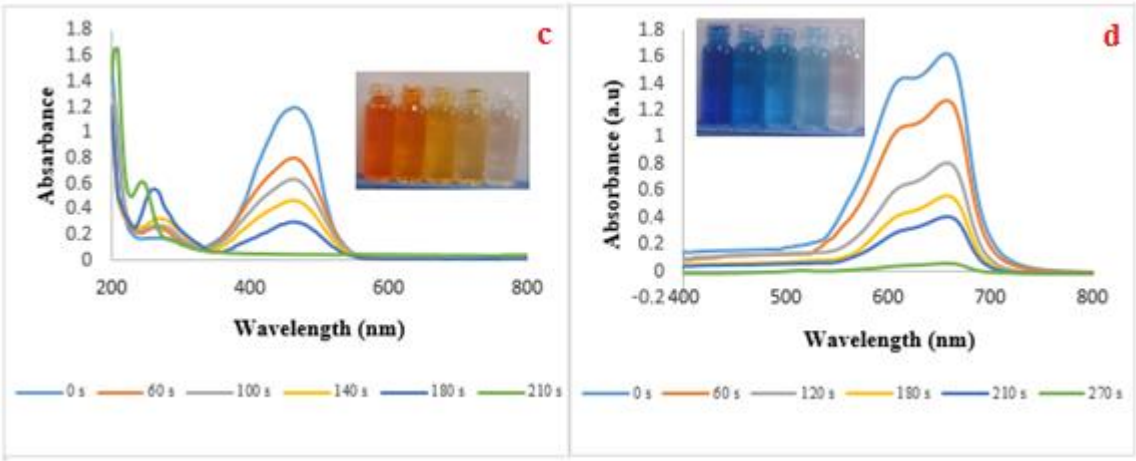

Figure 8: Reduction of MO (a) and MB (b) by different catalytic situations and time-dependent UV-Vis absorption spectra for the reduction of MO (c) and MB (d) by Fe_3O_4-Au@SF-SBA-15 nanoadsorbent in the presence of $NaBH_4$.

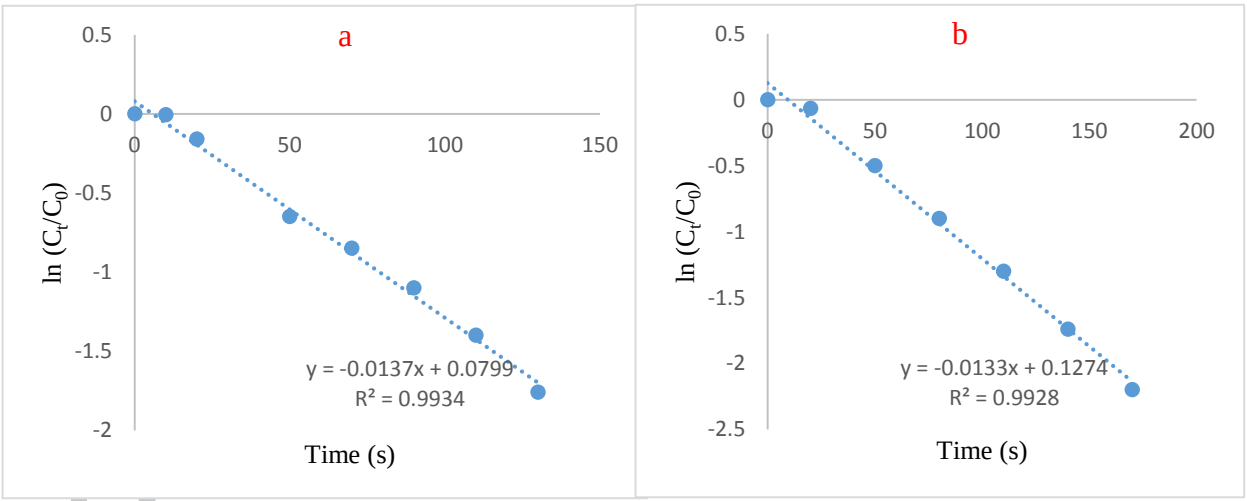

Figure 9: Kinetic curves for the reduction of MO (a) and MB (b) by Fe_3O_4-Au@SF-SBA-15 nanoadsorbent.

3.3. Mechanism of reduction of dyes by Fe_3O_4-Au@SF-SBA-15 nanoadsorbent

The catalyst composition has a significant effect on the catalyst activity [80]. In the reduction process of organic dyes, Au NPs supported on SF-SBA-15 surface serve as an electron relay system [81]. Scheme 2 shows the possible mechanism for reduction of organic dyes in the presence

of $NaBH_4$ by Au NPs. At the first step, the adsorption of dye molecules and BH_4^- occurs on the surface of adsorbent. In other words, dye molecules and BH_4^- first diffuse from the aqueous solution to SBA-15 and then, Au NPs immobilized on the SF-SBA-15 act as a catalyst to transfer electrons from BH_4^- to the organic dyes and these events lead to the reduction and decolorization of dye molecules.

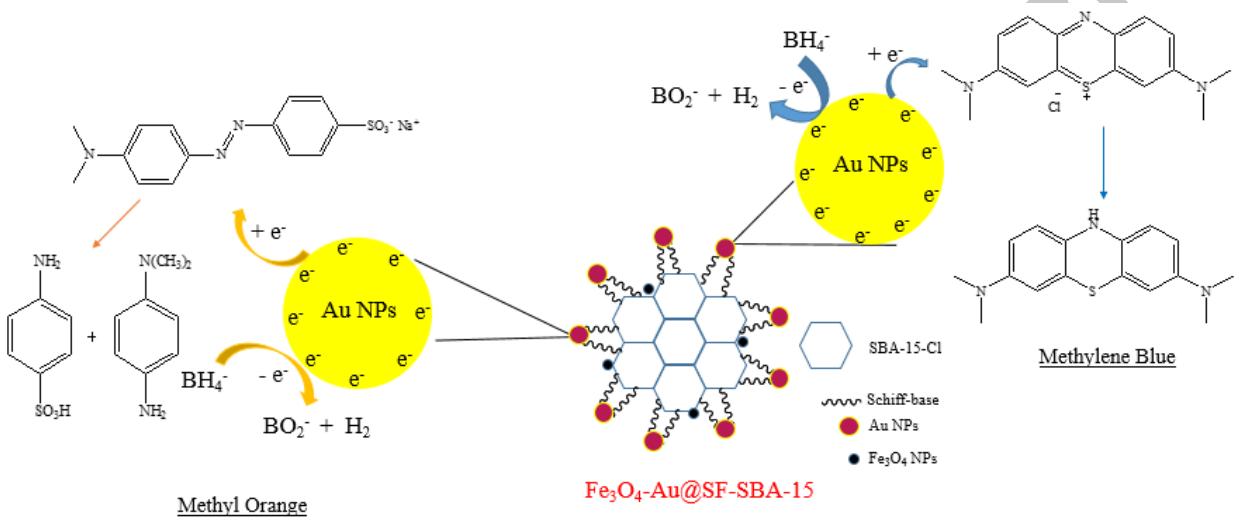

Scheme 2: Proposed mechanism for reduction of MO and MB in the presence of Fe_3O_4-Au@SF-SBA-15 and $NaBH_4$.

3.4. Evaluation of the catalytic activity in Suzuki-Miyaura coupling reaction

In order to evaluate the catalytic activity, the Fe_3O_4-Au@SF-SBA-15 nanocatalyst was used to synthesis biphenyl derivatives through Suzuki-Miyaura reaction. This catalytic system can catalyze Suzuki coupling reaction in a short time compare to Pd NPs. Moreover, Au NPs can efficiently catalyze the formation of C-C bond between less-reactive aryl halides (chlorobenzene) and phenylboronic acid. A comparison table for the evaluation of the efficiency of this catalytic system with Pd NPs presents in Table 3.

The model reaction for optimizing the effect of base, solvent, temperature and the amount of Au-loading is the coupling reaction between iodobenzene and phenylboronic acid. The results are available in Table 4. As can be seen, the nature of base strongly affects the efficiency of the coupling reaction (Table 3, entries 11-15) and K_2CO_3 afforded the best results for this reaction and

allowed the biphenyl product obtained in 98% yield after 45 min. The other bases such as NEt_3, NaOH, K_3PO_4 and NaOAc were not as effective as K_2CO_3 and only afforded moderate to low yields of the product. Another efficient factor on the catalytic performance of Fe_3O_4-Au@SF-SBA-15 is Au-loading (Table 4, entries 16-19). Based on the obtained results the best performance is obtained when 50 mg of catalyst (0.64 mmol% of Au) is used but in other cases, high yields of the C–C coupled products were not achieved. Finally, the effects of solvent and temperature were examined and the best result was obtained in H_2O: EtOH (1:1) at 80 °C for 45 min in the presence of 50 mg of Fe_3O_4-Au@SF-SBA-15 (0.64 mmol% of Au) using 2 mmol of K_2CO_3.

Entry 22 shows the role of magnetic nanoparticles in the coupling reaction. Based on the obtained results in the absence of magnetic NPs, there is no change in the yield of the production of biphenyl. Therefore, these nanoparticles would only help to easy separation of the catalyst from the reaction mixture.

We applied optimized reaction conditions for the coupling of aryl halides with phenylboronic acids. The results are available in Table 5.

Table 3: Suzuki coupling of chlorobenzene with phenylboronic acid catalyzed by a variety of catalysts.

Entry	Catalyst	Time (h)	Base	Temp. (°C)	Yield (%)	Ref.
1	Pd(II)–diimine complex	24	K_2CO_3	120	20	[82]
2	Pd–L/SBA-16	3	K_3PO_4	50	8	[83]
3	$[PdBr_2\{et(impy)\}_2]$	16	Cs_2CO_3	85	0	[84]
4	Pd(0)–MCM-41	24	K_2CO_3	80	24	[85]
5	Pd(II)–MCM-41	24	Na_2CO_3	60	60	[86]
6	Molecular sieves-supported Pd catalyst	18	K_2CO_3	120	84	[87]
7	Au@PATP	4	NaOH	80	87	[37]
8	Fe_3O_4-Au@SF-SBA-15	1.33	K_2CO_3	80	95	This work

L = 1,1,3,3-tetramethyl-2-(3-trimethoxysilylpropyl)-guanidine, et(impy) = ethylene bridged imidazo[1,5] pyridine-3-ylidenes, PATP = poly(2-aminothiophenol).

Table 4: Optimization of the reaction conditions.[a]

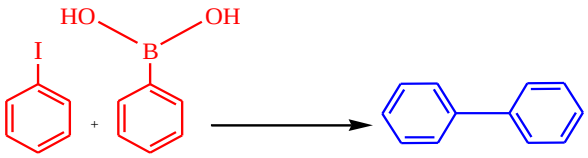

Entry	Catalyst	Solvent	Base	Au-Loading (mmol%)	Temp. (°C)	Time (min)	Yield[b] (%)
1	Fe_3O_4-Au@SF-SBA-15	toluene	K_2CO_3	0.64	reflux	300	11
2	Fe_3O_4-Au@SF-SBA-15	H_2O	K_2CO_3	0.64	reflux	100	54
3	Fe_3O_4-Au@SF-SBA-15	EtOH	K_2CO_3	0.64	reflux	100	41
4	Fe_3O_4-Au@SF-SBA-15	THF	K_2CO_3	0.64	reflux	300	13
5	Fe_3O_4-Au@SF-SBA-15	DMF	K_2CO_3	0.64	reflux	100	35
6	Fe_3O_4-Au@SF-SBA-15	DMF:H_2O (1:1)	K_2CO_3	0.64	100	100	56
7	Fe_3O_4-Au@SF-SBA-15	DMF:H_2O (2:1)	K_2CO_3	0.64	100	100	48
8	Fe_3O_4-Au@SF-SBA-15	DMF:H_2O (1:2)	K_2CO_3	0.64	100	100	63
9	Fe_3O_4-Au@SF-SBA-15	H_2O:EtOH (1:2)	K_2CO_3	0.64	80	45	81
10	Fe_3O_4-Au@SF-SBA-15	H_2O:EtOH (2:1)	K_2CO_3	0.64	80	45	89
11	Fe_3O_4-Au@SF-SBA-15	H_2O:EtOH (1:1)	K_2CO_3	0.64	80	45	98
12	Fe_3O_4-Au@SF-SBA-15	H_2O:EtOH (1:1)	NEt_3	0.64	80	45	78
13	Fe_3O_4-Au@SF-SBA-15	H_2O:EtOH (1:1)	NaOH	0.64	80	45	66
14	Fe_3O_4-Au@SF-SBA-15	H_2O:EtOH (1:1)	K_3PO_4	0.64	80	45	83
15	Fe_3O_4-Au@SF-SBA-15	H_2O:EtOH (1:1)	NaOAc	0.64	80	45	79
16	Fe_3O_4-Au@SF-SBA-15	H_2O:EtOH (1:1)	K_2CO_3	0.13	80	45	25
17	Fe_3O_4-Au@SF-SBA-15	H_2O:EtOH (1:1)	K_2CO_3	0.32	80	45	54
18	Fe_3O_4-Au@SF-SBA-15	H_2O:EtOH (1:1)	K_2CO_3	0.51	80	45	83
19	Fe_3O_4-Au@SF-SBA-15	H_2O:EtOH (1:1)	K_2CO_3	0.77	80	45	98
20	Fe_3O_4-Au@SF-SBA-15	H_2O:EtOH (1:1)	K_2CO_3	0.64	25	45	trace
21	Fe_3O_4-Au@SF-SBA-15	H_2O:EtOH (1:1)	K_2CO_3	0.64	50	45	57
22	Au@SF-SBA-15	H_2O:EtOH (1:1)	K_2CO_3	0.64	80	45	97

[a] Reaction conditions: iodobenzene (1 mmol), phenylboronic acid (1.2 mmol), base (2 mmol) and 5 mL of solvent.
[b] Isolated yield.

Table 5: Coupling of aryl halides with phenylboronic acid derivatives in the presence of catalytic amounts of Fe_3O_4-Au@SF-SBA-15.[a]

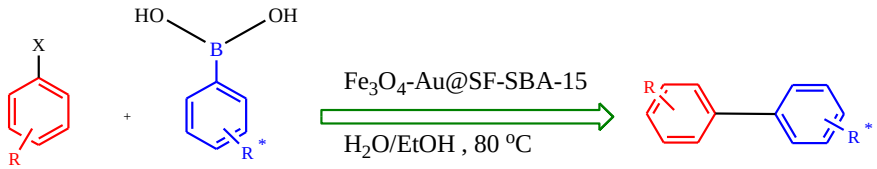

Entry	X	R	R*	Product	Time (min)	Yield[b] (%)	TOF[c] (h^{-1})
1	I	H	H	1a	45	98	204.16
2	Br	H	H	1a	60	97	151.56
3	Cl	H	H	1a	80	95	111.37
4	I	4-Me	H	1b	55	97	165.25
5	Br	4-Me	H	1b	60	94	146.88
6	Br	H	4-Me	1b	65	93	134.20
7	Cl	H	4-Me	1b	110	90	76.92
8	I	4-NO_2	H	1c	60	92	143.75
9	Cl	H	4-NO_2	1c	120	90	70.31
10	Br	4-NO_2	H	1c	75	94	117.5
11	I	4-OMe	H	1d	60	97	151.56
12	I	H	4-OMe	1d	65	94	135.64
13	Br	4-OMe	H	1d	70	95	127.18
14	I	4-COMe	H	1e	70	95	127.18
15	Cl	H	4-COMe	1e	150	87	54.38
16	I	4-OMe	4-OMe	1f	80	96	112.54
17	I	3,4-Dimethoxy	H	1g	60	93	145.31
18	I	2-Amino	H	1h	60	91	142.19

[a] Reaction conditions: aryl halide (1 mmol), phenylboronic acid (1.2 mmol), K_2CO_3 (2 mmol), H_2O:EtOH (5 mL) and 0.05 g of Fe_3O_4-Au@SF-SBA-15 (0.64 mmol% of Au).
[b] Isolated yields.
[c] TOF (turnover frequency) = (moles converted/mol of active site).(yield/ time).

3.5. Reusability of Fe_3O_4-Au@SF-SBA-15 nanocomposite

To examine the stability and recyclability of Fe_3O_4-Au@SF-SBA-15 nanoadsorbent, after each adsorption, we separated the adsorbent with a magnet, washed three times with distilled water and ethanol and then, reused for another color degradation reaction to evaluate its recycling performance. In addition, for investigating the catalytic performance of Fe_3O_4-Au@SF-SBA-15,

after the reaction between iodobenzene and phenylboronic acid, the catalyst separated by a magnet, washed three times with ethyl acetate and ethanol and then, reused for another coupling reaction.

As observed in Figure 10, the Fe_3O_4-Au@SF-SBA-15 nanoadsorbent can be successfully reused for fourteen times for adsorption of dye molecules and eight times for catalyzing the Suzuki-Miyaura coupling reaction (Figure 11) only with a very small loss in its catalytic activity. These results indicate the high stability of the Fe_3O_4-Au@SF-SBA-15 nanocomposite. A small decrease in its performance is due to the loss of catalyst after every recycling. After fourteen cycles for degradation of MB, the XRD peaks of the reused nanoadsorbent match well with the fresh nanocatalyst and it confirms the recoverability of the nanocomposite and stability of the Au NPs during the reaction (see Figure S5 in supporting information).

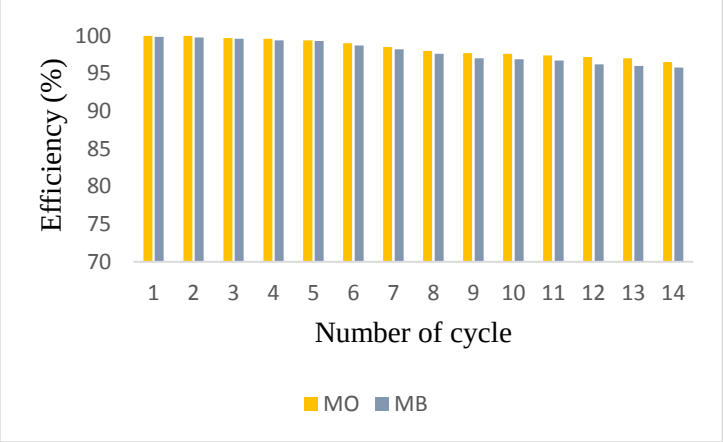

Figure 10: The reusability of Fe_3O_4-Au@SF-SBA-15 nanoadsorbent for degradation of MO and MB. (Reaction conditions for each cycle: $NaBH_4$ aqueous solution (2 mL, 0.25 M), aqueous solutions of MO or MB (18 mL, 50 ppm) and 1 mg of Fe_3O_4-Au@SF-SBA-15 nanoadsorbent (0.013 mmol% of Au).

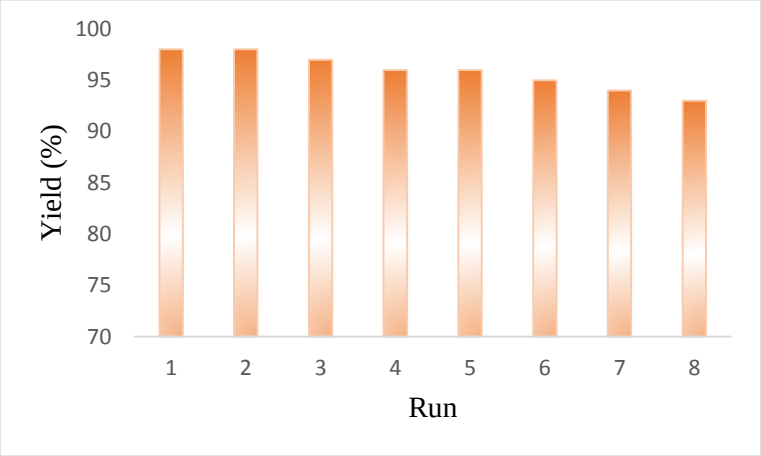

Figure 11: The reusability of Fe_3O_4-Au@SF-SBA-15 nanocatalyst for Suzuki-Miyaura coupling reaction between iodobenzene and phenylboronic acid. (Reaction conditions for each cycle: iodobenzene (1 mmol), phenylboronic acid (1.2 mmol), K_2CO_3 (2 mmol) and 0.05 g of Fe_3O_4-Au@SF-SBA-15 (0.64 mmol% of Au).

3.5.1. Leaching test

ICP analysis can evaluate the stability of the nanocomposite after several uses in reaction cycles. The ICP-OES results showed that only 0.05 wt% and 0.06 wt% of Au was leached after fourteen cycles for degradation of MO and MB, respectively and 0.04 wt% of Au was leached after eight cycles for the production of biphenyl. The results are available in Table 6.

Table 6: ICP analysis for determination of the amount of Au and Fe_3O_4 NPs after several reaction cycles

ICP results after fourteen cycles for degradation of MO		**ICP results after fourteen cycles for degradation of MB**		**ICP results after eight cycles for the production of biphenyl**	
Au (wt%)	Fe (wt%)	Au (wt%)	Fe (wt%)	Au (wt%)	Fe (wt%)
2.49	7.36	2.48	7.34	2.50	7.45

4. Conclusions

In this study, we introduced a green and economic method for the synthesis of Au NPs immobilized on SF-SBA-15 by *corn silk* extract. This nanocomposite successfully used for the degradation of the chemically and biologically resistant cationic (MB) and anionic (MO) dyes. The results exhibit that this heterogeneous composite can efficiently (>99%) degrade organic dyes within a short time. The reduction followed pseudo-first-order kinetics. Moreover, this nanocomposite can successfully catalyze the Suzuki-Miyaura coupling reaction between aryl halides and

phenylboronic acids. The biphenyl products obtained in excellent yields even for chlorobenzene derivatives at mild conditions. The unique characteristics of this nanocomposite include its simple and green preparation method, ease of separation, stability and recyclability. These features made it an excellent and sustainable adsorbent and catalyst in comparison with other systems. On the other hand, the high performance of this nanocomposite for degradation of various organic dyes, such as MO and MB indicates that this nanocomposite is also favorable for other dyes, potentiating its wide applications for industrial removal of dyes. Thus, it would be an ideal platform for the fabrication of highly efficient catalytic systems for various catalytic applications.

Acknowledgements

The authors gratefully acknowledge Razi University for the financial support.

References

[1] a) A. A. Ismail, D. W. Bahnemann, Mesostructured Pt/TiO2 nanocomposites as highly active photocatalysts for the photooxidation of dichloroacetic acid, J. Phys. Chem., 115 (2011) 5784-5791; b) A. A. Ismail, D. W. Bahnemann, J. Rathousky, V. Yarovyi, M. Wark, Multilayered ordered mesoporous platinum/titania composite films: does the photocatalytic activity benefit from the film thickness?, J. Mater. Chem., 21 (2011) 7802-7810.

[2] a) A. A. Ismail, D. W. Bahnemann, One-step synthesis of mesoporous platinum/titania nanocomposites as photocatalyst with enhanced photocatalytic activity for methanol oxidation, Green Chem., 13 (2011) 428-435; b) A. A. Ismail, D. W. Bahnemann, Mesoporous titania photocatalysts: preparation, characterization and reaction mechanisms, J. Mater. Chem., 21 (2011) 11686-11707.

[3] S. K. Ghosh, M. Mandal, S. Kundu, S. Nath, T. Pal, Bimetallic Pt–Ni nanoparticles can catalyze reduction of aromatic nitro compounds by sodium borohydride in aqueous solution, Appl. Catal. A: Gen., 268 (2004) 61-66.

[4] a) A. A. Ismail, D. W. Bahnemann, S. A. Al-Sayari, Synthesis and photocatalytic properties of nonocrystalline Au, Pd and Pt photodeposited onto mesoporous RuO_2-TiO_2 nanocomposites, Appl. Catal. A: Gen., 431 (2012) 62-68; b) A. A. Ismail, Facile synthesis of mesoporous Ag- loaded TiO_2 thin film and its photocatalytic properties, Microporous Mesoporous Mater., 149 (2012) 69-75; c) A. A. Ismail, T. A. Kandiel, D. W. Bahnemann, Novel (and better?) titania-based photocatalysts: brookite nanorods and mesoporous structures, J. Photochem. Photobiol. A: Chem., 216 (2010) 183-193.

[5] M. Brust, M. Walker, D. Bethell, D. J. Schiffrin, R. Whyman, Synthesis of thiol-derivatised gold nanoparticles in a two-phase liquid–liquid system, J. Chem. Soc. Chem. Commun., 7 (1994) 801-802.

[6] H. H. Huang, X. P. Ni, G. L. Loy, C. H. Chew, K. L. Tan, F. C. Loh, J. F. Deng, G. Q. Xu, Photochemical formation of silver nanoparticles in poly (N-vinylpyrrolidone), Langmuir, 12 (1996) 909-912.

[7] A. G. Boudjahem, S. Monteverdi, M. Mercy, M. M. Bettahar, Study of nickel catalysts supported on silica of low surface area and prepared by reduction of nickel acetate in aqueous hydrazine, J. Catal., 221 (2004) 325-334.

[8] S. Venkateswarlu, B. Natesh Kumar, B. Prathima, K. Anitha, N. V. V. Jyothi, A novel green synthesis of Fe_3O_4-Ag core shell recyclable nanoparticles using *Vitis viniferastem* extract and its enhanced antibacterial performance, Physica B: Condensed Matter., 457 (2015) 30-35.

[9] Z. Maksimović, D. Malenčić, N. Kovačević, Polyphenol contents and antioxidant activity of *Maydis stigma* extracts, Bioresource Technol., 96 (2005) 873-877.

[10] Anonymous. Cornsilk Tea Common Uses AND Benefits. Available online: http://www.cornsilktea.net (accessed on 13 April 2011).

[11] Anonymous. Corn Silk Tablet. Available online: http://www.nutritional-supplement-bible.com/cornsilk-tablets.html (accessed on 13 April 2011).

[12] M. A. Ebrahimzadeh, F. Pourmorad, S. Hafe, Antioxidant Activities of Iranian Corn Silk, Turk. J. Biol., 32 (2008) 43-49.

[13] Q. L. Hu, L. J. Zhang, Y. N. Li, Y. J. Ding, F. L. Li, Purification and anti-fatigue activity of flavonoids from corn silk, *Int. J. Phys. Sci., 5 (***2010**) 321-326.

[14] J. W. Bastien, Pharmacopeia of qollahuayaandeans, J. Ethnopharmacol., 8 (1982) 97-111.

[15] A. Caceres, L. M. Giron, A. M. Martinez, Diuretic activity of plants used for the treatment of urinary ailments in Guatemala, J. Ethnopharmacol., 19 (1987) 233-245.

[16] D. D. Dat, N. N. Ham, D. H. Khac, N. T. Lam, P. T. Son, N. V. Dau, M. Grabe, R. Johansson, G. Lindgren, N. E. Stjernstrom, Studies on the individual and combined diuretics effects of four Vietnamese traditional herbal remedies (*Zea mays*, *Imperatacylindrica*, *Plantago major* and *Orthosiphonstamineus*), J. Ethnopharmacol., 36 (1992) 225-231.

[17] F. Grases, J. G. March, M. Ramis, A. Costa-Bauzá, The influence of *Zea mays* on urinary risk factors for kidney stones in rats, Phytother. Res., 7 (1993) 146-149.

[18] E. Yesilada, G. Honda, E. Sevik, M. Tabata, T. Fujita, T. Tanaka, Y. Takeda, Y. Takaishi, Traditional medicine in Turkey. V. Folk medicine in the inner Taurus Mountains, J. Ethnopharmacol., 46 (1995) 133-152.

[19] V. Steenkamp, Phytomedicines for the prostate, Fitoterapia, 74 (2003) 545-552.

[20] M. A. Ebrahimzadeh, M. Mahmoudi, N. Ahangar, S. Ehteshami, F. Ansaroudi, S. F. Nabavi, S. M. Nabavi, Antidepressant activity of corn silk, Pharmacologyonline, 3 (2009) 647-652.

[21] D. V. O. Velazquez, H. S. Xavier, J. E. M. Batista, C. D. Castro-Chaves, *Zea mays* L. extracts modify glomerular function and potassium urinary excretion in conscious rats, Phytomedicine, 12 (2005) 363-369.

[22] Z. A. Maksimovic, N. Kovačević, Preliminary assay on the antioxidative activity of *Maydis stigma* extracts, Fitoterapia, 74 (2003) 144-147.

[23] H. Bai, C. Hai, M. Xi, X. Liang, R. Liu, Protective Effect of Maize Silks (*Maydis stigma*) Ethanol Extract on Radiation-Induced Oxidative Stress in Mice, Plant Food Hum. Nutr.,

56 (2010) 271-276.

[24] G. Sepehri, A. Derakhshanfar, F. Y. Zade, Protective effects of corn silk extract administration on gentamicin-induced nephrotoxicity in rat, Comp. Clin. Pathol., 20 (2011) 89-94.

[25] W. I. Wan Rosli, A. R. Nurhanan, S. S. J. Mohsin, C. G. Farid, Aqueous, alcoholic treated and proximate analysis of maydis stigma (*Zea mays* hairs), Ann. Microsc., 8 (2008) 66-72.

[26] J. Liu, S. Lin, Z. Wang, C. Wang, E. Wang, Y. Zhang, J. Liu, Supercritical fluid extraction of flavonoids from *Maydis stigma* and its nitrite-scavenging ability, Food Bioprod. Process, 89 (2011) 333-339.

[27] M. Haruta, When gold is not noble: catalysis by nanoparticles, Chem. Rec., 3 (2003) 75-87.

[28] A. Abad, P. Concepción, A. Corma, H. García, A collaborative effect between gold and a support induces the selective oxidation of alcohols, Angew. Chem., Int. Ed., 44 (2005) 4066-4069.

[29] N. Thielecke, M. Aytemir, U. Drusse, Selective oxidation of carbohydrates with gold catalysts: Continuous-flow reactor system for glucose oxidation, Catal. Today, 121 (2007) 115-120.

[30] D. Zim, V. R. Lando, J. Dupont, A. L. Monteiro, $NiCl_2$ $(PCy_3)_2$: A simple and efficient catalyst precursor for the Suzuki cross-coupling of aryl tosylates and arylboronic acids, Org. Lett., 3 (2001) 3049-3051.

[31] M. B. Thathagar, J. Beckers, G. Rothenberg, Copper-catalyzed Suzuki cross-coupling using mixed nanocluster catalysts, J. Am. Chem. Soc., 124 (2002) 11858-11859.

[32] C. Gonzalez-Arellano, A. Corma, M. Iglesias, F. Sanchez, Gold (I) and (III) catalyze Suzuki cross-coupling and homocoupling, respectively, J. Catal., 238 (2006) 497-501.

[33] M. K. Dalal, Green chemistry on solid support, Procedia Comput. Sci., 3 (2012) 276-280.

[34] N. Kudo, M. Perseghini, G. C. Fu, A versatile method for Suzuki cross-coupling reactions of nitrogen heterocycles, Angew. Chem., Int. Ed., 45 (2006) 1282-1306.

[35] M. T. Reetz, E. Westermann, Phosphane-free palladium-catalyzed coupling reactions: the decisive role of Pd nanoparticles, Angew. Chem., Int. Ed., 39 (2000) 165-168.

[36] Y. Wang, Z. Liu, B. Han, Z. Sun, Y. Huang, G. Yang, Facile synthesis of polyaniline nanofibers using chloroaurate acid as the oxidant, Langmuir, 21 (2005) 833-836

[37] J. Han, Y. Liu, R. Guo, Facile synthesis of highly stable gold nanoparticles and their unexpected excellent catalytic activity for Suzuki− Miyaura cross-coupling reaction in water, J. Am. Chem. Soc., 131 (2009) 2060-2061.

[38] M. P. Sk, C. K. Jana, A. Chattopadhyay, A gold–carbon nanoparticle composite as an efficient catalyst for homocoupling reaction, Chem. Commun., 49 (2013) 8235-8237

[39] S. K. Movahed, M. Fakharian, M. Dabiri, A. Bazgir, Gold nanoparticle decorated reduced graphene oxide sheets with high catalytic activity for Ullmann homocoupling, Rsc Adv., 4 (2014) 5243-5247.

[40] T. X. Bui, H. Choi, Adsorptive removal of selected pharmaceuticals by mesoporous silica SBA-15, J. Hazard Mater., 168 (2009) 62-68.

[41] M. Anbia, S. Amirmahmoodi, Adsorption of phenolic compounds from aqueous solutions using functionalized SBA-15 as a nano-sorbent, Sci. Iran., 18 (2011) 446-452.

[42] H. Yan, P. Lu, Z. Pan, X. Wang, Q. Zhang, L. Li, Ce/SBA-15 as a heterogeneous ozonation catalyst for efficient mineralization of dimethyl phthalate, J. Mol. Catal. A: Chem., 377 (2013) 57-64.

[43] E. Da'na, A. Sayari, Optimization of copper removal efficiency by adsorption on amine-modified SBA-15: experimental design methodology, Chem. Eng. J., 167 (2011) 91-98.

[44] a) M. Ghaedi, M. Pakniat, Z. Mahmoudi, S. Hajati, R. Sahraei, A. Daneshfar, Synthesis of nickel sulfide nanoparticles loaded on activated carbon as a novel adsorbent for the competitive removal of Methylene blue and Safranin-O, Spectrochim. Acta. Mol.

Biomol., 123 (2014) 402-409; b) M. Ghaedi, N. Zeinali, A. M. Ghaedi, M. Teimuori, J. Tashkhourian, Artificial neural network-genetic algorithm based optimization for the adsorption of methylene blue and brilliant green from aqueous solution by graphite oxide nanoparticle, Spectrochim. Acta. Mol. Biomol., 125 (2014) 264-277; c) M. Ghaedi, A. Ansari, M. H. Habibi, A. R. Asghari, Removal of malachite green from aqueous solution by zinc oxide nanoparticle loaded on activated carbon: Kinetics and isotherm study, J. Ind. Eng. Chem., 20 (2014) 17-28.

[45] X. Wang, G. Zhu, F. Guo, Removal of uranium (VI) ion from aqueous solution by SBA-15, Ann. Nucl. Energy, 56 (2013) 151-157.

[46] G. R. Bardajee, R. Malakooti, I. Abtin, H. Atashin, Palladium Schiff-base complex loaded SBA-15 as a novel and pyridopyrazine derivatives, Microporous Mesoporous Mater., 169 (2013) 67-74.

[47] J. R. Anacona, J. L. Rodriguez, J. Camus, Synthesis, characterization and antibacterial activity of a Schiff base derived from cephalexin and sulphathiazole and its transition metal complexes, Spectrochim. Acta. Mol. Biomol., 129 (2014) 96-102.

[48] B. Shafaatian, A. Soleymanpour, N. K. Oskouei, B. Notash, S. A. Rezvani, Synthesis, crystal structure, fluorescence and electrochemical studies of a new tridentate Schiff base ligand and its nickel (II) and palladium (II) complexes, Spectrochim. Acta. Mol. Biomol., 128 (2014) 363-369.

[49] P. K. Saha, S. Saha, S. Koner, Chromotropism of Cr (salen) moiety in zeolite matrix: synthesis, characterization and catalytic activity study of Cr (salen)-NaY hybrid catalyst, J. Mol. Catal. A: Chem., 203 (2003) 173-178.

[50] K. Dhara, K. Sarkar, D. Srimani, S. K. Saha, P. Chattopadhyay, A. Bhaumik, A new functionalized mesoporous matrix supported Pd (II)-Schiff base complex: an efficient catalyst for the Suzuki–Miyaura coupling reaction, Dalton Trans., 39 (2010) 6395-6402.

[51] L. Dolatyari, M. R. Yaftian, S. Rostamnia, Removal of uranium (VI) ions from aqueous solutions using Schiff base functionalized SBA-15 mesoporous silica materials, J. Environ. Manage., 169 (2016) 8-17.

[52] Y. Qin, H. Ren, F. Zhu, L. Zhang, C. Shang, Z. Wei, M. Luo, Preparation of POSS-based organic–inorganic hybrid mesoporous materials networks through Schiff base chemistry, Eur. Polym. J., 47 (2011) 853-860.

[53] D. Zhao, Q. Huo, J. Feng, B. F. Chmelka, G. D. Stucky, Nonionic triblock and star diblock copolymer and oligomeric surfactant syntheses of highly ordered, hydrothermally stable, mesoporous silica structures, J. Am. Chem. Soc., 120 (1998) 6024-6036.

[54] D. Zhao, J. Sun, Q. Li, G. D. Stucky, Morphological control of highly ordered mesoporous silica SBA-15, Chem. Mater., 12 (2000) 275-279.

[55] E. Vunain, R. Malgas-Enus, K. Jalama, R. Meijboom, The effect of recrystallization time on pore size and surface area of mesoporous SBA-15, J. Sol-Gel Sci. Technol., 68 (2013) 270-277.

[56] D. Pérez-Quintanilla, I. del Hierro, M. Fajardo, I. Sierra, Mesoporous silica functionalized with 2-mercaptopyridine: synthesis, characterization and employment for Hg (II) adsorption, Microporous and Mesoporous Mater., 89 (2006) 58-86.

[57] M. M. Khodaei, M. Dehghan, Synthesis and characterization of Co_3O_4 immobilized on dipeptide-functionalized silica-coated magnetite nanoparticles as a catalyst for the selective aerobic oxidation of alcohols, New J. Chem. 2018. Doi: 10.1039/c8nj00781k.

[58] a) S. Chala, K. Wetchakun, S. Phanichphant, B. Inceesungvorn, N. Wetchakun, Enhanced visible-light- response photocatalytic degradation of methylene blue on Fe-loaded $BiVO_4$ photocatalyst, J. Alloys Compd., 597 (2014) 129-135; b) T. L. Spires-Jones, T. Friedman, R. Pitstick, M. Polydoro, A. Roe, G. A. Carlson, B. T. Hyman, Methylene blue does not reverse existing neurofibrillary tangle pathology in the rTg4510 mouse model of tauopathy, Neurosci. Lett., 562 (2014) 63-68.

[59] T. Yang, C. M. Shen, H. J. Gao, Highly ordered self-assembly with large area of Fe_3O_4 nanoparticles and the magnetic properties, J. Phys. Chem. B, 109 (2005) 23233-23236.

[60] C. Pecharroman, T. Gonzalez-Carreno, J. E. Iglesias, The infrared dielectric properties of maghemite, γ-Fe_2O_3, from reflectance measurement on pressed powders, Phys. Chem. Miner., 22 (1995) 21-29.

[61] V. K. Tomer, R. Malik, S. Jangra, S. P. Nehra, S. Duhan, One pot direct synthesis of mesoporous SnO_2/SBA-15 nanocomposite by the hydrothermal method, Mat. Lett., 132 (2014) 228-230.

[62] D. Zhao, Q. Huo, J. Feng, B. F. Chmelka, G. D. Stucky, Nonionic triblock and star diblock copolymer and oligomeric surfactant syntheses of highly ordered, hydrothermally stable, mesoporous silica structures, J. Am. Chem. Soc., 120 (1998) 6024-6036.

[63] P. Borah, Y. Zhao, β-Diketimine appended periodic mesoporous organosilica as a scaffold for immobilization of palladium acetate: An efficient green catalyst for Wacker type reaction, J. Catal., 318 (2014) 43-52.

[64] K. Hasanudin, P. Hashim, S. Mustafa, Corn silk (Stigma maydis) in healthcare: a phytochemical and pharmacological review, Molecules, 17 (2012) 9697-9715.

[65] S. Trifunschi, M. F. Munteanu, V. Agotici, S. Pintea, R. Gligor, Determination of flavonoid and polyphenol compounds in Viscum album and Allium Sativum extracts, Int. Curr. Pharm. J., 4 (2015) 382-385.

[66] S. Brunauer, L. S. Deming, W. E. Deming, E. Teller, On a Theory of the van der Waals Adsorption of Gases, J. Am. Chem. Soc., 62 (1940) 1723-1732.

[67] J. Morere, M. J. Tenorio, M. J. Torralvo, C. Pando, J. A. R. Renuncio, A. Cabanas, Deposition of Pd into mesoporous silica SBA-15 using supercritical carbon dioxide, J. Supercrit. Fluids, 56 (2011) 213-222.

[68] a) H. Yan, P. Lu, Z. Pan, X. Wang, Q. Zhang, L. Li, Ce/SBA-15 as a heterogeneous ozonation catalyst for efficient mineralization of dimethyl phthalate, J. Mol. Catal. A: Chem., 377 (2013) 57-64; b) E. Da'na, A. Sayari, Optimization of copper removal efficiency by adsorption on amine-modified SBA-15: experimental design methodology, Chem. Eng. J., 167 (2011) 91-98.

[69] W. Haiss, N. Thanh, J. Aveyard, D. Fernig, Determination of size and concentration of gold nanoparticles from UV−Vis spectra, Anal. Chem., 79 (2007) 4215-4221.

[70] M. Kruk, M. Jaroniec, C. H. Ko, R. Ryoo, Characterization of the Porous Structure of SBA-15, Chem. Mater., 12 (2000) 1961-1968.

[71] P. Saikia, A. B. U. T MIAH, P. P. Das, Highly efficient catalytic reductive degradation of various organic dyes by Au/CeO_2-TiO_2 nano-hybrid, J. Chem. Sci., 129 (2017) 81-93.

[72] B. R. Ganapuram, M. Alle, R. Dadigala, A. Dasari, V. Maragoni, V. Guttena, Catalytic reduction of methylene blue and Congo red dyes using green synthesized gold nanoparticles capped by salmalia malabarica gum, Int. Nano Lett., 5 (2015) 215-222.

[73] R. S. S. Siddhardha, V. L. Kumar, A. Kaniyoor, V. S. Muthukumar, S. Ramaprabhu, R. Podila, A. M. Rao, S. S. Ramamurthy, Synthesis and characterization of gold graphene composite with dyes as model substrates for decolorization: A surfactant free laser ablation approach, Spectrochim. Acta A, 133 (2014) 365-371.

[74] J. Li, C. Y. Liu, Y. Liu, Au/graphene hydrogel: synthesis, characterization and its use for catalytic reduction of 4-nitrophenol, J. Mater. Chem., 22 (2012) 8426-8430.

[75] M. M. Khan, J. Lee, M. H. Cho, Au@TiO_2 nanocomposites for the catalytic degradation of methy orange and methylene blue: An electron relay effect, J. Ind. Eng. Chem., 20 (2014) 1584-1590.

[76] T. Yao, T. Cui, H. Wang, L. Xu, F. Cui, J. Wu, A simple way to prepare Au@polypyrrole/Fe_3O_4 hollow capsules with high stability and their application in catalytic reduction of methylene blue dye, Nanoscale, 6 (2014) 7666-7674.

[77] S. Megarajan, K. B. A. Ahmed, G. R. K. Reddy, P. S. Kumar, V. Anbazhagan, Phytoproteins in green leaves as building blocks for photosynthesis of gold nanoparticles: An efficient electrocatalyst towards the oxidation of ascorbic acid and the reduction of hydrogen peroxide, J. Photochem. Photobiol. B, 155 (2016) 7-12.

[78] a) B. K. Ghosh, S. Hazra, B. Naik, N. N. Ghosh, Preparation of Cu nanoparticle loaded SBA-15 and their excellent catalytic activity in reduction of variety of dyes, Powder Technol., 269 (2015) 371-378; b) M. M. Khan, J. Lee, M. H. Cho, Au@ TiO_2 nanocomposites for the catalytic degradation of methyl orange and methylene blue: An electron relay effect, J. Ind. Eng. Chem., 20 (2014) 1584-1590; c) S. He, Z. Fei, L. Li, B. Sun, X. Feng, W. Ji, Synthesis and catalytic activity of M@ SiO_2 (M= Ag, Au and Pt) nanostructures via “core to shell” and “shell then core” approaches, Chin. J. Catal., 34

(2013) 2098-2109; d) Z. Y. Zhang, C. L. Shao, P. Zou, P. Zhang, M. Y. Zhang, In situ assembly of well-dispersed gold nanoparticles on electrospun silica nanotubes for catalytic reduction of 4-nitrophenol, Chem. Commun., 47 (2011) 3906-3908; e) U. P. Azad, V. Ganesan, M. Pal, Catalytic reduction of organic dyes at gold nanoparticles impregnated silica materials: influence of functional groups and surfactants, J. Nanopart. Res., 13 (2011) 3951-3959; f) Q. Wang, Y. Li, B. Liu, Q. Dong, G. Xu, L. Zhang, J. Zhang, Novel recyclable dual-heterostructured Fe_3O_4@ CeO_2/M (M= Pt, Pd and Pt–Pd) catalysts: synergetic and redox effects for superior catalytic performance, J. Mater. Chem. A, 3 (2015) 139-147; g) Z. Gan, A. Zhao, M. Zhang, W. Tao, H. Guo, Q. Gao, R. Mao, E. Liu, Controlled synthesis of Au-loaded Fe_3O_4@ C composite microspheres with superior SERS detection and catalytic degradation abilities for organic dyes, Dalton Trans., 42 (2013) 8597-8605.

[79] a) S. C. Tang, S. Vongehr, X. K. Meng, Controllable incorporation of Ag and Ag–Au nanoparticles in carbon spheres for tunable optical and catalytic properties, J. Mater. Chem., 20 (2010) 5436-5445; b) H. L. Jiang, T. Akita, T. Ishida, M. Haruta, Q. Xu, Synergistic catalysis of Au@ Ag core− shell nanoparticles stabilized on metal− organic framework, J. Am. Chem. Soc., 133 (2011) 1304-1306.

[80] a) K. Mallick, M. Witcomb, M. Scurrell, Silver nanoparticle catalysed redox reaction: an electron relay effect, Mater. Chem. Phys., 97 (2006) 283-287; b) S. K. Ghosh, S. Kundu, M. Mandal, T. Pal, Silver and gold nanocluster catalyzed reduction of methylene blue by arsine in a micellar medium, Langmuir, 18 (2002) 8756-8760.

[81] a) A. K. Patra, A. Dutta, A. Bhaumik, Cu nanorods and nanospheres and their excellent catalytic activity in chemoselective reduction of nitrobenzenes, Catal. Commun., 11 (2010) 651-655; b) R. K. Sharma, Y. Monga, A. Puri, Magnetically separable silica@ Fe_3O_4 core–shell supported nano-structured copper (II) composites as a versatile catalyst for the reduction of nitroarenes in aqueous medium at room temperature, J. Mol. Catal. A, 393 (2014) 84-95; c) J. Feng, L. Su, Y. H. Ma, C. L. Ren, Q. Guo, X. G. Chen, $CuFe_2O_4$ magnetic nanoparticles: A simple and efficient catalyst for the reduction of nitrophenol, Chem. Eng. J., 221 (2013) 16-24.

[82] J. Zhou, X. Guo, C. Tu, X. Li, H. Sun, Aqueous Suzuki coupling reaction catalyzed by water-soluble diimine/Pd (II) systems, J. Organomet. Chem., 694 (2009) 697-702.

[83] H. Yang, X. Han, Z. Ma, R. Wang, J. Liu, X. Ji, Palladium-guanidine complex immobilized on SBA-16: a highly active and recyclable catalyst for Suzuki coupling and alcohol oxidation, Green Chem., 12 (2010) 441-451.

[84] M. Nonnenmacher, D. Kunz, F. Rominger, T. Oeser, Palladium (II) complexes bearing methylene and ethylene bridged pyrido-annelated N-heterocyclic carbene ligands as active catalysts for Heck and Suzuki–Miyaura cross-coupling reactions, J. Organomet. Chem., 692 (2007) 2554-2563.

[85] S. Jana, S. Haldar, S. Koner, Heterogeneous Suzuki and Stille coupling reactions using highly efficient palladium (0) immobilized MCM-41 catalyst, Tetrahedron Lett., 50 (2009) 4820-4823.

[86] S. Bhunia, R. Sen, S. Koner, Anchoring of palladium (II) in chemically modified mesoporous silica: An efficient heterogeneous catalyst for Suzuki cross-coupling reaction, Inorganica Chim. Acta, 363 (2010) 3993-3999.

[87] R. Dey, B. Sreedhar, B.C. Ranu, Molecular sieves-supported palladium (II) catalyst: Suzuki coupling of chloroarenes and an easy access to useful intermediates for the synthesis of irbesartan, losartan and boscalid, Tetrahedron, 66 (2010) 2301-2305.

A Green and Cost-Effective Approach for the Production of Gold Nanoparticles Using *Corn Silk* Extract: A Recoverable Catalyst for Suzuki-Miyaura Reaction and Adsorbent for Removing of Dye Pollutants

Mohammad Mehdi Khodaei,[a,b]* Mahsa Dehghan[a]

[a] Department of Organic Chemistry, Razi University, Kermanshah 67149-67346, Iran.

[b] Nanoscience & Nanotechnology Research Center (NNRC), Razi University, Kermanshah 67149-67346, Iran

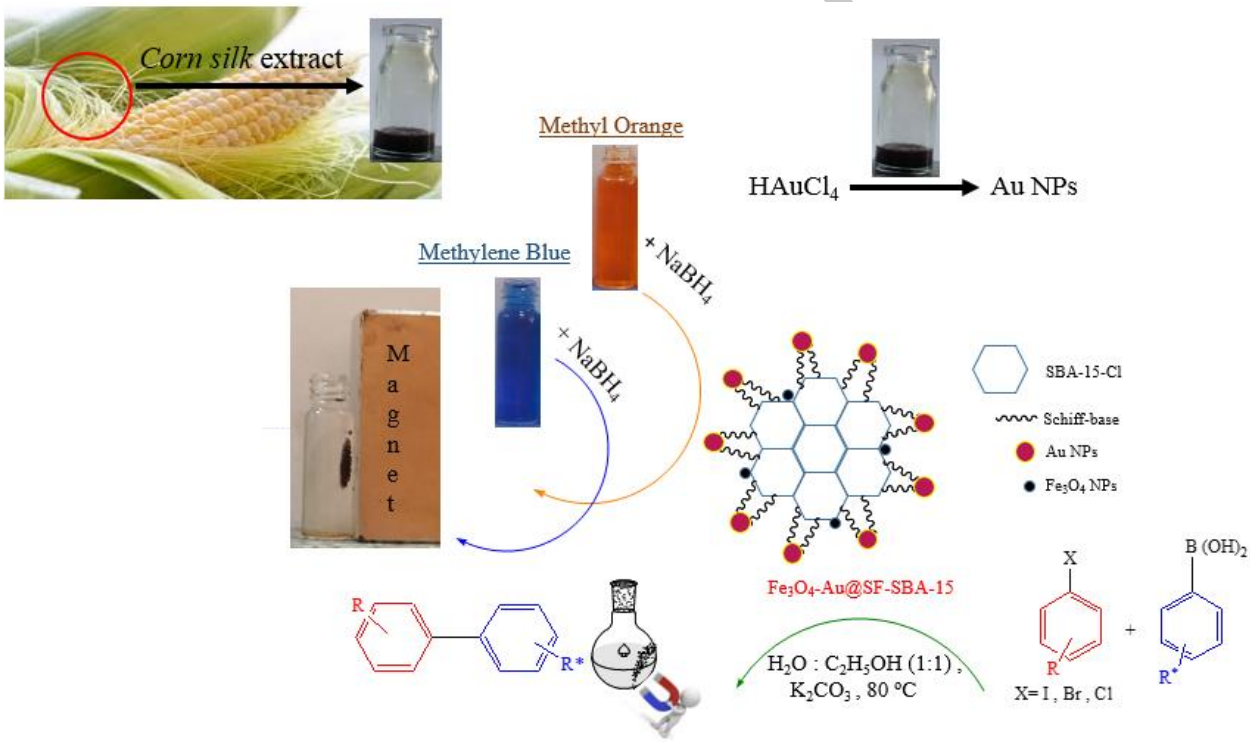

Effective reduction of dye pollutants and synthesis of biphenyl products in good yields at mild conditions by using of Au NPs synthesized by a green and cost-effective method

Highlights:

- Green and cost-effective synthesis of Au nanoparticles was performed using *corn silk* extract.
- The catalytic performance was evaluated for the degradation of organic dyes and Suzuki-Miyaura coupling reaction.
- Under optimum condition, the decolorization efficiency was >99% and biphenyl products were obtained in excellent yields at mild condition.
- The developed method is a fast and inexpensive method with ease of separation and high reusability.